Spectroscopic Properties of Spheroidene Analogs Having Different Extents of π-Electron Conjugation

Harry A. Frank,*,†,‡ Ruel Z. B. Desamero,† Veeradej Chynwat,† Ronald Gebhard,§ Ineke van der Hoef,§ Frans Jos Jansen,§ Johan Lugtenburg,*,§ David Gosztola,|| and Michael R. Wasielewski*,||,⊥

Department of Chemistry, 215 Glenbrook Road, University of Connecticut, Storrs, Connecticut 06269-4060, Gorlaeus Laboratories, Leiden University, 2300 RA Leiden, The Netherlands, Chemistry Division, Argonne National Laboratories, Argonne, Illinois 60439, and Department of Chemistry, Northwestern University, Evanston, Illinois 60208

Received: August 6, 1996; In Final Form: October 25, 1996[⊗]

The spectroscopic properties of spheroidene and a series of spheroidene analogs with extents of π-electron conjugation ranging from 7 to 13 carbon−carbon double bonds were studied using steady-state absorption, fluorescence, fluorescence excitation, and time-resolved absorption spectroscopy. The spheroidene analogs studied here were 5′,6′-dihydro-7′,8′-didehydrospheroidene, 7′,8′-didehydrospheroidene, and 1′,2′-dihydro-3′,4′,7′,8′-tetradehydrospheroidene and taken together with data from 3,4,7,8-tetrahydrospheroidene, 3,4,5,6-tetrahydrospheroidene, 3,4-dihydrospheroidene already published (DeCoster, B.; Christensen, R. L.; Gebhard, R.; Lugtenburg, J.; Farhoosh, R.; Frank, H. A. *Biochim. Biophys. Acta* **1992**, *1102*, 107) provide a systematic series of molecules for understanding the molecular features that control energy transfer to bacteriochlorophyll in photosynthetic bacterial light-harvesting complexes. All of the molecules were purified by high-pressure liquid chromatographic techniques prior to the spectroscopic experiments. The absorption spectra of the molecules were observed to red-shift with increasing extent of π-electron conjugation. The room temperature fluorescence data show a systematic crossover from dominant $S_1 \rightarrow S_0$ ($2^1A_g \rightarrow 1^1A_g$) emission to dominant $S_2 \rightarrow S_0$ ($1^1B_u \rightarrow 1^1A_g$) with increasing extent of conjugation. The S_2 fluorescence quantum yields of all the carotenoids in the series were measured here and indicate that 3,4-dihydrospheroidene with nine carbon−carbon double bonds has an S_2 quantum yield of $(2.7 \pm 0.3) \times 10^{-4}$ which is the highest value in the series. The lifetimes of the S_1 states of the molecules were determined from time-resolved transient absorption spectroscopy and found to decrease as the conjugated chain length increases. The transient data are discussed in terms of the energy gap law for radiationless transitions which allows a prediction of the S_1 energies of the molecules. The implications of these results for the process of light harvesting by carotenoids in photosynthesis are discussed.

Introduction

Carotenoids supplement the light-capturing ability of chlorophyll in antenna pigment−protein complexes by harvesting light in the ∼425−500 nm visible region where chlorophyll is not an efficient absorber.[1,2] The energy is then transferred from the carotenoids to chlorophyll via singlet state energy transfer. Several different mechanisms describing energy transfer have been advanced.[3−7] Which of these mechanisms is most appropriate to describe the rate and efficiency of energy transfer between carotenoids and chlorophylls will depend on the distance between the donor and acceptor molecules and the nature of the excited states involved in the process. Thus, an in-depth understanding of the energy state complexion of carotenoids is essential for detailing the manner in which these molecules participate in light harvesting in photosynthesis.

Carotenoids possess two low-lying excited electronic states, denoted S_1 and S_2, that play important roles in energy transfer in photosynthesis.[1,8,9] The ground state, denoted S_0, and S_1 of *all-trans*-polyenes possess A_g symmetry in the idealized C_{2h} point group. Electronic transitions between these states, *i.e.* $S_0 \rightarrow S_1$ ($1^1A_g \rightarrow 2^1A_g$) absorption or $S_1 \rightarrow S_0$ ($2^1A_g \rightarrow 1^1A_g$) fluorescence, are symmetry forbidden. In contrast, electronic transitions to and from S_0 and the second excited state, S_2, which has B_u symmetry, *i.e.* the transitions $S_0 \rightarrow S_2$ ($1^1A_g \rightarrow 1^1B_u$) absorption and $S_2 \rightarrow S_0$ ($1^1B_u \rightarrow 1^1A_g$), are allowed. The $S_0 \rightarrow S_2$ ($1^1A_g \rightarrow 1^1B_u$) transition is responsible for the characteristic strong absorption associated with all polyenes in the visible region. Carotenoids, owing to their large extents of substitution by functional groups, do not adhere strictly to C_{2h} symmetry. However, because carotenoids possess many of the spectral characteristics of the parent polyenes from which they were derived, the same symmetry designations described above are used when referring to carotenoids as well as polyenes.

The photophysics and photochemistry of many short polyenes have been studied extensively.[8−11] Yet, it remains unclear precisely how to take the conclusions drawn from the data on polyenes and apply them to the behavior of carotenoid molecules.[12,13] Also, the relationships between the energies and decay dynamics of excited states of carotenoids and the molecular details of how carotenoids carry out their light-harvesting role in photosynthetic systems need to be elucidated.[14] An investigation by Andersson *et al.*[15] of the energies and decay times of the S_1 and S_2 states of β-carotene and analogous compounds having 5, 7, 8, 9, 15, and 19 conjugated double bonds have shown that the S_1 lifetimes decrease with increasing extent of π-electron conjugation. Similar observations were

† University of Connecticut.
‡ Fax: 860−486−3772. E-mail: frank@uconnvm.uconn.edu.
§ Leiden University.
|| Argonne National Laboratories.
⊥ Northwestern University.
⊗ Abstract published in *Advance ACS Abstracts,* December 15, 1996.

S1089-5639(96)02373-0 CCC: $14.00

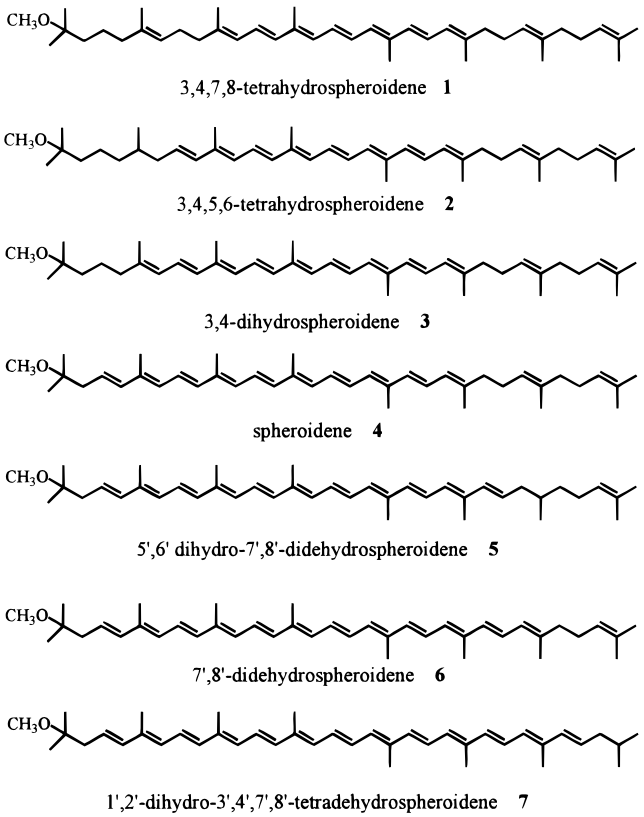

Figure 1. Molecular structures of spheroidene and its analogs.

reported for spheroidene analogs having 7, 8, 9, and 10 carbon−carbon double bonds.[12,13]

The present work extends the study of the photophysics and photochemistry of spheroidene by examining the absorption, fluorescence, fluorescence excitation, fluorescence quantum yields, and transient absorption dynamics of 5′,6′-dihydro-7′,8′-didehydrospheroidene (**5**), 7′,8′-didehydrospheroidene (**6**), and 1′,2′-dihydro-3′,4′,7′,8′-tetradehydrospheroidene (**7**). These are a systematic series of spheroidene analogs possessing 11, 12, and 13 conjugated carbon−carbon double bonds, respectively (Figure 1). Taken together with data already published[12,13] on spheroidene (**4**) and its shorter analog compounds, 3,4,7,8-tetrahydrospheroidene (**1**), 3,4,5,6-tetrahydrospheroidene (**2**), 3,4-dihydrospheroidene (**3**), having 7, 8, and 9 carbon−carbon double bonds, and their S_2 fluorescence quantum yields reported here for the first time, the molecular features that control the ability of carotenoids to carry out their light-harvesting function in photosynthesis are beginning to emerge.

Materials and Methods

Preparation and Purification of the Samples. Spheroidene was obtained from anaerobically grown *Rhodobacter sphaeroides* wild type strain 2.4.1 cells by extraction with acetone and partitioning with pentane. After the pentane was evaporated and redissolved in acetone, the sample was loaded onto a DEAE sephacel column that was equilibrated with acetone. A mixture of carotenoids, primarily spheroidene and spheroidenone, was then eluted from the column using acetone. Spheroidene was separated from the other carotenoids using an alumina column with 0.25, 0.5, and 1% ethyl acetate in petroleum ether solutions as stepwise eluants. The synthesis and purification of 3,4,7,8-tetrahydrospheroidene, 3,4,5,6-tetrahydrospheroidene, and 3,4-dihydrospheroidene have been previously described.[16] The synthesis and purification of 5′,6′-dihydro-7′,8′-didehydrospheroidene, 7′,8′-didehydrospheroidene, and 1′,2′-dihydro-3′,4′,7′,8′-tetradehydrospheroidene will be reported in detail elsewhere.[17]

High-Pressure Liquid Chromatography (HPLC) Analysis. The solvent from the purified carotenoid solutions was evaporated using a stream of gaseous nitrogen, and the solid carotenoids were redissolved in methanol. HPLC analysis and separation of the carotenoids were carried out using a Waters 996 liquid chromatograph equipped with a photodiode array detector and employing a Nova Pak C_{18} (4 μm particle size) Waters reversed-phase column (3.9 × 350 mm) and a Lichrosorb RP-18 (5 μm particle size) Phenomenex guard column (4.0 × 30 mm). The samples were eluted at a flow rate of 1.0 mL/min with a mobile phase programmed as follows: 0−12 min, isocratic methanol/acetonitrile (95/5 v/v); 12−27 min, linear gradient to methanol/*n*-hexane (95/5 v/v); 27−45 min, linear gradient to methanol/acetonitrile (95/5 v/v). The major peaks in each chromatogram were independently collected.

Absorption and Fluorescence Spectral Analysis. After HPLC the carotenoid solutions were dried using a stream of gaseous nitrogen and redissolved in *n*-hexane. Fluorescence and fluorescence excitation spectra of these samples were then done on a SLM 8000C (SLM Instruments, Inc.) spectrofluorimeter. A 450 W ozone-free xenon arc lamp and a 1500 grooves per mm grating monochromator comprised the variable-wavelength excitation light system. The sample emission passed through a 10 mm Glan-Thompson calcite prism-type vertical polarizer to reduce Wood's anomaly, through an appropriate glass cutoff filter depending on the sample, and into another monochromator positioned 90° to the excitation beam. The intensity of both the incident and emitted light were detected by two separate Hamamatsu model R-928 photomultiplier tubes. The contributions to the emission spectra resulting from the Raman scattering bands of the solvent were corrected by subtracting a solvent blank taken under identical conditions. The fluorescence spectra were also corrected for the wavelength dependencies of the optical components using a correction factor generated by scanning the excitation and emission monochromators synchronously. Fluorescence excitation spectra were obtained in ratio mode with Rhodamine 800 in ethylene glycol as the reference. A Milton Roy spectronic 3000 array spectrometer (SLM-Aminco) was used to obtain the absorption spectra. All determinations were done at room temperature.

Quantum Yield Measurements. The fluorescence quantum yields of 3,4,7,8-tetrahydrospheroidene, 3,4,5,6-tetrahydrospheroidene, and 3,4-dihydrospheroidene were measured relative to perylene in cyclohexane ($\phi_F = 0.94$).[18] Rhodamine 590 in methanol ($\phi_F = 0.95$)[19] was used for 5′,6′-dihydro-7′,8′-didehydrospheroidene, 7′,8′-didehydrospheroidene, and 1′,2′-dihydro-3′,4′,7′,8′-tetradehydrospheroidene. Both perylene in cyclohexane and rhodamine 590 in methanol were used for spheroidene. The evaluation of the quantum yields was based on the following equation[20]

$$\phi_c = \phi_r\left(\frac{1-10^{-A_r\lambda}}{1-10^{-A_c\lambda}}\right)\left(\frac{I_{r\lambda}}{I_{c\lambda}}\right)\left(\frac{n_c^2}{n_r^2}\right)\left(\frac{D_c}{D_r}\right) \quad (1)$$

where ϕ_c and ϕ_r are the quantum yields of the carotenoid and reference solutions, respectively. $I_{c\lambda}$ and $I_{r\lambda}$ are the relative intensities of the exciting light at wavelength λ for the carotenoid and standard solutions. $A_{c\lambda}$ and $A_{r\lambda}$ are the optical densities of the carotenoid and standard solutions at wavelength λ. n_c is the refractive index of *n*-hexane and is equal to 1.375 06 at 20 °C, and n_r is the refractive index of methanol (1.3288 at 20 °C) or cyclohexane (1.426 62 at 20 °C). D_c and D_r are the integrated areas of the corrected emission spectra of the carotenoid and standard solutions.

Transient Absorption Measurements. All of the carotenoids were dissolved in diethyl ether and placed in 1 cm path

length cuvettes. Following deoxygenation of the samples by bubbling with nitrogen gas, the cuvettes were sealed. The transient absorption apparatus used to measure the excited state lifetime consists of a homemade, self-mode-locked, Ti:sapphire oscillator that was pumped by the 5 W all lines output from an Ar^+ laser (Laser Ionics 1400).[21] The Ti:sapphire oscillator emits 25 fs, 800 nm pulses at a 97 MHz repetition rate with an average power of 400 mW. The 25 fs pulses from the oscillator are temporally stretched using a double-passed grating/mirror combination to a duration of 200 ps. These chirped pulses were amplified in a homemade Ti:sapphire regenerative amplifier that employed a folded cavity and used an acoustooptical modulator (NEOS N13389) for injection and cavity dumping. The regenerative amplifier was pumped by an intracavity frequency-doubled, Q-switched, Nd:YAG laser (Laser Applications 9560) that produced 540 μJ, 700 ns, 532 nm pulses at a 24 kHz repetition rate. The output of the Ti:sapphire regenerative amplifier was recompressed with 50% efficiency using a single transmission grating (Kaiser Optical Systems) to give 33 μJ, 70 fs, 800 nm pulses. Using appropriate beam splitters, about 3 μJ of 800 nm light was used to generate a very smooth white light continuum by focusing it with a 5 cm lens into a 3 mm thick block of sapphire. Shot-to-shot intensity fluctuations of the probe beam were generally less than 2%. The remaining 800 nm light was frequency-doubled with 25% efficiency using a 1 mm long LBO type I crystal to yield 100 fs, 400 nm pulses.

The energy of the blue excitation light on the sample was varied using a polarizer-$^{\lambda}/_{2}$ wave plate combination. The polarization of the pump beam was set to the magic angle with respect to the probe beam. Typically, <500 nJ was used to excite the molecules. The excitation beam was chopped at 635 Hz synchronized to the laser repetition rate using a quartz acoustooptic beam deflector (INTRA ACTION ASM-703-8). The arrival of the excitation beam relative to the probe beams was accomplished with an optical delay line that used a linear stepping motor (Compumotor) with 1 μ (7 fs) resolution. The nearly collinear and codirectional excitation and measuring probe beams were focused into the sample to ca. 0.3 mm diameter. The sample was contained in a 1 cm path length cuvette and was stirred. The wavelengths of the measuring and reference probe beams were selected with a SPEX M270 monochromator. Changes in the transmission of the measuring probe light through the sample and changes in the reference probe beam were monitored by photomultiplier tubes (Hamamatsu H5783-01). The output of each PMT was digitized using a sample and hold amplifier and 12-bit A/D board (National Instruments) and was recorded with a personal computer (Gateway 66 MHz 486). The data acquisition software monitored the quality of each shot and only averaged shots within 5% of the average intensity of the reference probe beam level. Kinetic parameters were obtained by iterative reconvolution using the Levenberg−Marquardt algorithm. The instrumental time response was 100 fs at 400 nm.

Results

HPLC Analysis and Purification of Geometric Isomers. Figure 2 shows the HPLC chromatogram of 5′,6′-dihydro-7′,8′-didehydrospheroidene (11 carbon−carbon double bonds) which is typical of spheroidene and all the analogs studied here. The retention times of the carotenoids on the reverse-phase column were very similar, with the most intense peak eluting after about 30 min. The absorption spectra corresponding to the major chromatographic peaks for each sample were dominated by a distinctive, strongly allowed transition with extensive vibronic structure in the 400−500 nm region. For 5′,6′-dihydro-7′,8′-didehydrospheroidene (Figure 2) the longest wavelength vibrational feature of this transition appears at approximately 500 nm. In addition to the prominent absorption in the 400−500 nm region, the absorption spectra corresponding to the other peaks in the HPLC chromatogram show varying intensities of absorption at approximately 360 nm. These so-called "*cis*-peaks" which usually occur at ∼140 nm to shorter wavelength of the red-most spectral feature in the absorption spectrum indicate that the other compounds eluting from the column in this time domain are different geometric isomers of the same carotenoid. The *all-trans*-isomer is distinguished because it is characterized by the smallest cis-peak in the mixture. In all cases, the concentration of the all-*trans*-carotenoid was dominant in the mixture. This is presumably because it is also known to be the most stable of the geometric isomers.[22]

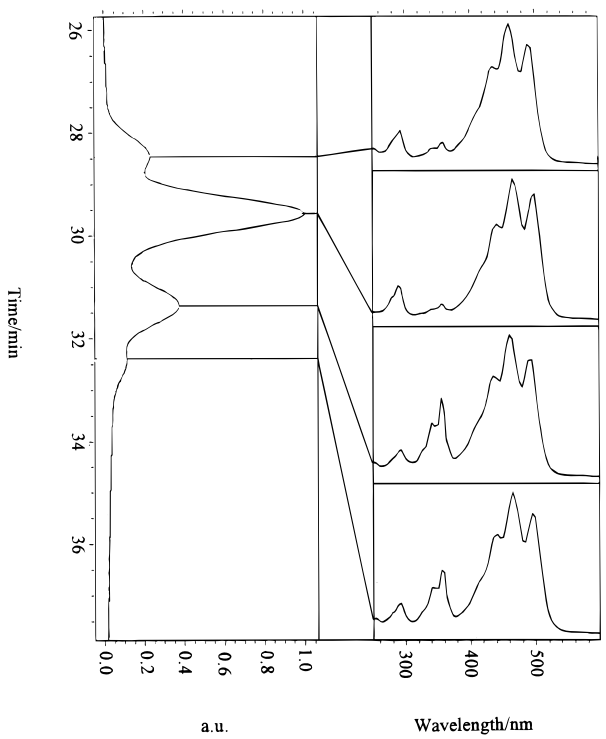

Figure 2. HPLC chromatogram (left-hand side) and corresponding spectra (right-hand side) of 5′,6′-dihydro-7′,8′-didehydrospheroidene (**5**) which are typical of the chromatograms for spheroidene and all the analogs studied. The chromatogram was detected using absorption at 467 nm.

In addition to resolving the various major peaks, the HPLC procedure separated species with shorter elution times. These fractions absorb at wavelengths less than 400 nm, and most likely are less conjugated polyenes consisting primarily of degradation products of the carotenoids that were not eliminated by the initial column purification steps. These impurities which have high fluorescence yields can affect the fluorescence and the fluorescence excitation spectra. The present HPLC protocol removed them from the samples used in the measurements reported here.

Absorption and Fluorescence Spectral Analysis. The absorption spectra for spheroidene and the six analog compounds in *n*-hexane are shown in Figure 3. The spectra are red-shifted as the extent of the π-conjugation increases. The absorption spectra correspond to the $S_0 \rightarrow S_2$ ($1^1A_g \rightarrow 1^1B_u$) transitions. Hence, the red-shifting of the spectra indicates a decreasing trend in the energy difference between S_2 and S_0. For the spectra for all the molecules in the series, the full width at half-height of the individual vibronic bands was ∼1000 cm^{-1} and the widths of the entire $S_0 \rightarrow S_2$ ($1^1A_g \rightarrow 1^1B_u$) absorption spectral profiles

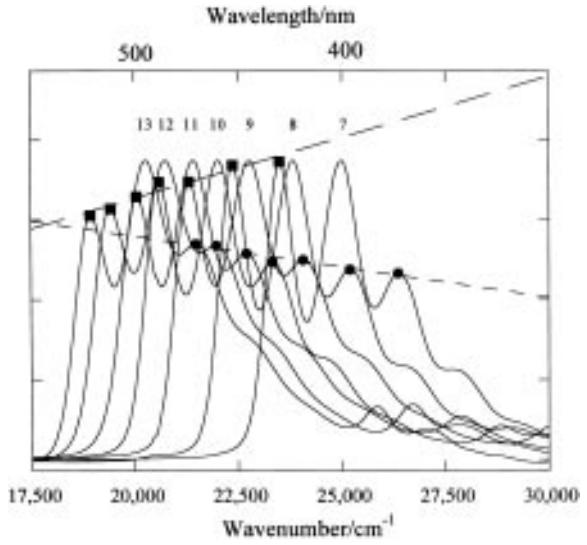

Figure 3. Absorption spectra of spheroidene and the six analog compounds. The spectra are red-shifted with increasing extents of π-electron conjugation and show the variations in the relative intensities of the vibronic bands. The intensity of the lowest energy vibronic feature decreases with the extent of π-electron conjugation (— ■ —), whereas that of the higher energy vibronic feature increases with the extent of π-electron conjugation (— ● —). The corresponding number of conjugated double bonds are indicated directly above the wavelength of maximum absorption, λ_{max}, for each of the molecules.

were 3680 ± 30 cm^{-1}. The relative intensities of the vibronic bands of the carotenoids changed noticeably with the extent of π-electron conjugation. This is evident from the sloped dashed lines in Figure 3 which show that by normalizing the intensities of the spectra at their respective wavelengths of maximum absorption, the λ_{max} values, one of the higher energy vibronic features is observed to increase in intensity as the extent of conjugation increases. The intensity of the lowest energy vibronic feature in the absorption spectrum, the spectral origin, decreases in intensity with increasing extent of conjugation.

Figure 4 shows the room temperature fluorescence, fluorescence excitation and absorption spectra for spheroidene (10 carbon−carbon double bonds) and the analogs with 11, 12, and 13 carbon−carbon double bonds. The spectra for the short chain spheroidene analogs, *i.e.* analogs with less than 10 carbon−carbon double bonds, have been published previously.[12] The fluorescence spectra of the longer chromophore carotenoids appear for the most part as mirror images of their $S_0 \rightarrow S_2$ absorptions. The small Stokes shifts between the origins of emission and absorption suggest that the emission from all these molecules corresponds to the $S_2 \rightarrow S_0$ ($1^1B_u \rightarrow 1^1A_g$) transition. There was no evidence for any longer wavelength, $S_1 \rightarrow S_0$ ($2^1A_g \rightarrow 1^1A_g$) emission originating from any of the molecules with 10 or more carbon−carbon double bonds. The fluorescence excitation spectra, also shown in Figure 4, were monitored at the wavelength of maximum intensity of the emission profiles. These excitation spectra correspond well to the absorption spectra and, therefore, support the assignment of the fluorescence profiles to spheroidene and the analogs. As seen in their absorption spectra, the fluorescence and fluorescence excitation spectra red-shift with increasing extents of π-electron conjugation. The energies of the S_2 states of spheroidene and its analogs were determined from the intersections of their absorption and fluorescence spectra. These values are given in the last column of Table 1.

Transient Absorption Experiments. Excitation of the molecules with a 120 fs laser pulse results in a rapid buildup

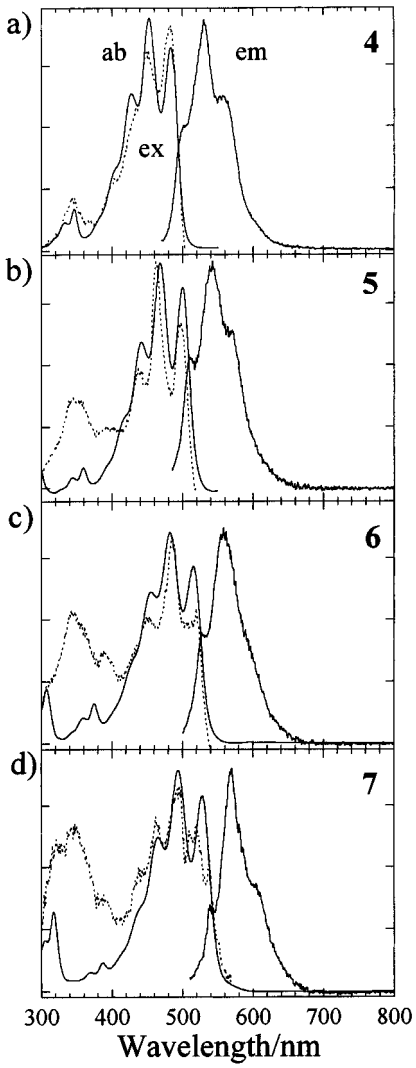

Figure 4. Room temperature absorption (ab, —), fluorescence (em, —), and fluorescence excitation (ex, - - -) spectra of molecules (a) **4**, (b) **5**, (c) **6**, and (d) **7** in *n*-hexane. The fluorescence spectra were obtained by exciting at the wavelength where the absorption is maximum for the compound. The fluorescence excitation spectra were obtained by monitoring at the wavelength where the emission is maximum for the compound.

of their $S_1 \rightarrow S_n$ absorption bands probed using a white light continuum. These absorption bands subsequently decay with single-exponential kinetics to zero as shown in Figure 5. The S_1 lifetimes determined from these data are 8.7 ± 0.1 ps for spheroidene (compound **4**), 3.9 ± 0.1 ps for 5′,6′-dihydro-7′,8′-didehydrospheroidene (compound **5**), 2.7 ± 0.1 ps for 7′,8′-didehydrospheroidene (compound **6**), and 1.1 ± 0.2 ps for 1′,2′-dihydro-3′,4′,7′,8′-tetradehydrospheroidene (compound **7**). The S_1 lifetimes of 3,4,7,8-tetrahydrospheroidene, 3,4,5,6-tetrahydrospheroidene, and 3,4-dihydrospheroidene have been previously determined[13] and are summarized with the present data in Table 1.

In accord with the energy gap law for radiationless transitions,[23] the trend toward decreasing S_1 lifetime implies that the energy difference between S_1 and S_0 decreases as the extent of conjugation increases.[13,15,21,24−26] Because carotenoids deactivate primarily nonradiatively (quantum yields of emission $<3 \times 10^{-4}$, see below), their S_1 energies can be deduced from a fit of the dynamics of the $S_1 \rightarrow S_0$ transition to the energy gap law given as

TABLE 1: S_1 Lifetimes and S_1 and S_2 Energies of Spheroidene and Its Analogs[a]

carotenoid		S_1 lifetimes/ps	S_1 energies/cm^{-1}	S_2 energies/cm^{-1}
3,4,7,8-tetrahydrospheroidene	**1**	407 ± 23[b]	18 400[c]	23 200 ± 500
3,4,5,6-tetrahydrospheroidene	**2**	85 ± 5[b]	16 700[c]	22 300 ± 500
3,4-dihydrospheroidene	**3**	25.4 ± 0.9[b]	15 300[c]	21 300 ± 500
spheroidene	**4**	8.7 ± 0.1[b]	14 200 ± 50	20 600 ± 400
5′,6′-dihydro-7′,8′-didehydrospheroidene	**5**	3.9 ± 0.1	13 245 ± 50	19 700 ± 400
7′,8′-didehydrospheroidene	**6**	2.7 ± 0.1	12 805 ± 60	19 000 ± 400
1′,2′-dihydro-3′,4′,7′,8′-tetradehydrospheroidene	**7**	1.1 ± 0.2	11 775 ± 200	18 400 ± 300

[a] Unless otherwise indicated the S_1 energies were deduced from a fit of the dynamics of the $S_1 \rightarrow S_0$ transition to the energy gap law. The uncertainties in the numbers were propagated from the precisions in the determinations of the S_1 lifetimes. The S_2 energies of spheroidene and its analogs were determined from the intersections of their absorption and fluorescence spectra as described in the text. Their uncertainties were estimated as ±10 nm from the point of intersection. [b] From Frank et al.[10] [c] From DeCoster et al.[9]

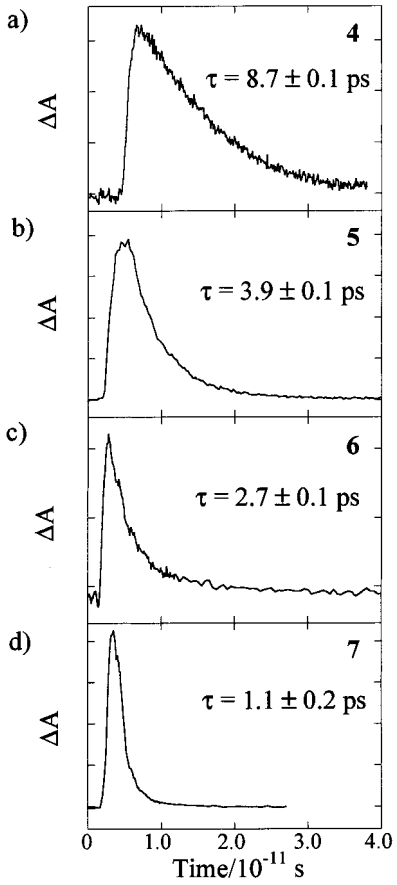

Figure 5. Decay of the transient absorbance excited at 420 nm and probed at 520 nm for compound **4**, 545 nm for compound **5**, 555 nm for compound **6**, and 590 nm for compound **7**. The probe wavelengths correspond to the maxima of the $S_1 \rightarrow S_n$ absorption. The *y*-axis expresses the change in absorption, ΔA, in arbitrary units. τ is the S_1 state lifetime.

$$k_{ic}(S_1 \rightarrow S_0) = \frac{C^2(2\pi)^{1/2}}{\hbar(\Delta E \hbar\omega_M)^{1/2}} \exp\left(-\gamma \frac{\Delta E}{\hbar\omega_M}\right) \qquad (2)$$

where $k_{ic}(S_1 \rightarrow S_0)$ is the internal conversion rate constant for the radiationless deactivation of the S_1 state. For the carotenoids studied here, this is very well approximated by the reciprocal of the measured S_1 lifetime. ΔE is the $S_1 - S_0$ ($2^1A_g - 1^1A_g$) energy difference, C is a vibronic coupling matrix element, $\hbar\omega_M$ is the energy of the accepting vibrational mode, $\gamma = \ln(2\Delta E/d\Delta^2_M\hbar\omega_M) - 1$, and can be related to the relative displacement, Δ_M, of the potential surfaces of the S_1 and S_0 electronic states, and d is the number of degenerate modes. A series of seven carotenoids for which both the dynamics and energies of the S_1 states are known simultaneously from transient absorption and fluorescence data were used to derive a theoretical curve describing the dependence of the dynamics of the $S_1 \rightarrow S_0$ transition on the energy separation between the states. This curve is shown in Figure 6. The normal acceptor modes for carotenoids are the C−C stretching modes where $h\omega_M$ is in the range 1300−1600 cm^{-1}.[27] The data presented in Figure 6 was then used to deduce the S_1 energies of spheroidene and its long-chain analogs from the dynamics of their $S_1 \rightarrow S_0$ transitions. These energies along with those from the short-chain spheroidene analogs published previously are summarized in Table 1 and plotted in Figure 7 along with the energies of the S_2 states. Similar to what is observed for the S_2 states, the energies of the S_1 states follow a decreasing trend with extent of π-electron conjugation. However, the rate of decrease in energy with chain length is faster for the S_1 states than for the S_2 states. Hence, the energy gap between S_2 and S_1 increases from 4800 to 6625 cm^{-1} as the π-electron conjugated chain length increases from 7 to 13 carbon−carbon double bonds.

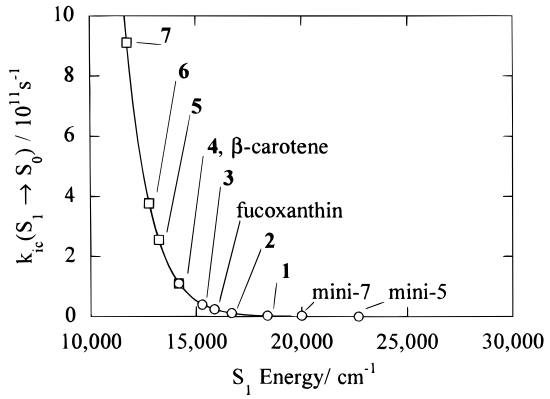

Figure 6. Fit of the energy gap law equation to the dynamics and energetics data from three spheroidene analogs, compounds **1**, **2**, and **3**, β-carotene, and two of its analogs mini-5 and mini-7, having 5 and 7 carbon−carbon double bonds, respectively (open circles). From the curve (solid line) generated from a fit of eq 2 to these data (open circles), the energies of the S_1 states of compounds **4**, **5**, **6**, and **7** (open squares) were deduced. The values of these energies are given in Table 1.

Quantum Yield Measurements. The S_2 emission yields for spheroidene and its analogs were evaluated according to the expression given in eq 1. The data are summarized in Table 2 and plotted in Figure 8. The results show that as the π-electron conjugated chain length increases from 7 to 9 carbon−carbon double bonds, the S_2 fluorescence quantum yield increases, reaching a maximum value for 3,4-dihydrospheroidene of (2.7 ± 0.3) × 10^{-4} as the highest in the series. As the extent of π-electron conjugation is increased from 9 to 13 carbon−carbon double bonds, the S_2 fluorescence quantum yield decreases. (See Table 2 and Figure 8.) The error bars in Figure 8 represent the uncertainties calculated from the standard deviations from the mean values of at least two trials, and, in each trial, the emission at two or more wavelengths of excitation was measured. The values for the S_2 quantum yields of spheroidene ((1.2 ± 0.25)

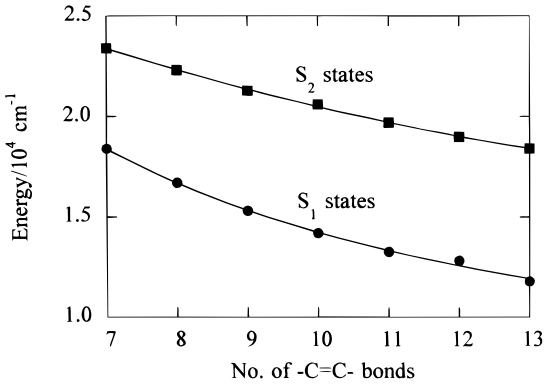

Figure 7. Energies of the S_1 and S_2 states of spheroidene and the six analog compounds plotted against the number of −C═C− double bonds. The energies are fitted (solid lines) using the function $A + B/(N + C)$ where *A*, *B*, and *C* are adjustable parameters and *N* is the number of double bonds in the molecule. The best fit for the plot of the S_1 state energies was derived using values $A = 3802$ cm^{-1}, $B = 1.1 \times 10^5$ cm^{-1}, and $C = 0.500$. The S_2 state energies were best fit using the parameters $A = 10\,955$ cm^{-1}, $B = 1.1 \times 10^5$ cm^{-1}, and $C = 2.020$.

$\times 10^{-4}$) and 3,4-dihydrospheroidene ($(2.7 \pm 0.3) \times 10^{-4}$) measured here are within the limits of error of the $(2.0 \pm 1.0) \times 10^{-4}$ and $(2.2 \pm 1.0) \times 10^{-4}$ values reported by Cogdell *et al.*[28] for spheroidene and neurosporene, respectively. Neurosporene, like 3,4-dihydrospheroidene, has nine carbon−carbon double bonds. Also, the value reported here for the quantum yield of 5′,6′-dihydro-7′,8′-didehydrospheroidene ($(0.62 \pm 0.20) \times 10^{-4}$) which contains 11 carbon−carbon double bonds is very close to the value of $(0.8 \pm 0.4) \times 10^{-4}$ observed by Cogdell *et al.*[28] for lycopene which has the same extent of π-electron conjugation.

Discussion

Absorption and Fluorescence Spectra. The major features of the absorption and fluorescence spectra for the series of spheroidene analog molecules remain relatively constant over the series; the full widths at half-height of the individual vibronic bands and the widths of the entire absorption line shapes remained essentially constant for all the molecules in the series. The relative intensities of the vibronic bands of the carotenoids did change, however, as a function of the number of carbon−carbon double bonds. This is evident from the sloped dashed lines drawn in Figure 3. The higher energy vibronic features are observed to increase in intensity as the extent of conjugation increases, whereas the intensity of the lowest energy vibronic feature, the spectral origin, in the absorption spectrum decreases in intensity with increasing extent of conjugation. For the shortest molecule in the series, 3,4,7,8-tetrahydrospheroidene, which has seven carbon−carbon double bonds, the spectral origin is roughly equivalent in intensity to the second vibronic component. The variation in the intensities of the vibronic bands is most likely attributable to a shift in the equilibrium position of the S_2 excited state potential energy surface relative to that of the ground state. The absorption spectral observations are consistent with the relative displacement between the minima of the S_0 and S_2 excited state surfaces increasing as the extent of π-electron conjugation increases. An increase in the relative displacement between the S_0 and S_2 excited state surfaces would lead to a gradual shift of the Franck−Condon maximum of the transition from the red-most absorption band, the spectral origin, to higher vibronic features, as is observed.

The Lifetimes and Energies of the S_1 States. The transient data presented in Table 1 for spheroidene and its analogs show that the S_1 lifetimes become shorter as the extent of conjugation is increased. This is consistent with the energy gap between S_1 and S_0 decreasing with increasing conjugated chain length. Thus, as mentioned above, a fit of the energy gap law given in eq 2 to a set of data for which the energies and lifetimes of carotenoids are simultaneously known can be used to predict the S_1 energies (Figure 6). This is done by extrapolating the fitted curve to obtain the S_1 energies of the longer chromophore carotenoids from which no fluorescence from their S_1 states is able to be detected. It is important to point out that this type of extrapolation provides only estimates of the S_1 energies. However, the very low emission quantum yields, the very fast lifetimes of the states, and the physically reasonable values of the parameters used in the fit justify the determination.

Figure 7 shows that the energies of both the S_1 and S_2 states of the spheroidene analogs decrease as the extent of conjugation increases and that the energies would level off for conjugated chain lengths greater than 13 carbon−carbon double bonds. This convergence was also observed in model polyene[29] and in β-carotene analogs.[15,24] A simple description of the effect was advanced by Kohler[29] utilizing Hückel theory and employing alternating resonance integrals to achieve bond alternation. The model used only four configurations: the 1^1A_g ground state, the 1^1B_u excited singlet state, a double-excitation configuration, and a symmetric linear combination of two double-jump excitations. The calculation neglected all but the configuration interaction between the nearly degenerate latter configurations and assigned the mixing matrix element for these states to a term having the functional form $A + B/(N + C)$, where *A*, *B*, and *C* are adjustable parameters and *N* is the number of double bonds in the molecule. This form of the perturbation requires the state energies to vary inversely with increasing extent of conjugation. The result is that the energies of the states reach a finite limit as the chain length is increased. With this model a reasonable prediction for the excited state energies of several polyenes was achieved.[29] The parameters *A* and *B* were assigned the same values regardless of whether the polyene chain was unsubstituted or terminally substituted at both ends with phenyl groups (α,ω-diphenylpolyenes) or alkyl chains (α,ω-dialkylpolyenes). *N* varied between 3 and 8 double bonds. The parameter *C* was used to correct for the effects of the terminal functional groups on electron correlation. *C* was set to zero for the calculations on linear unsubstituted polyenes.[29]

Andersson and Gillbro[24] applied this model to extrapolate the excitation energies of several long-chain β-carotene analogs to the long-chain limit. These authors explored the effect of empirically fitting their spectral data to several different functional forms of the mixing matrix element, but following Kohler[29] they found that a two-term, $A + B/N$ function was sufficient to describe the behavior of most of the series of β-carotene analogs with the exception of those having 15 and 19 carbon−carbon double bonds for which an additional C/N^2 term was required to achieve a satisfactory fit.[24]

The data presented in Figure 7 for the spheroidene analogs are well fit by the $A + B/(N + C)$ expression. The parameters obtained from the fit were $A = 3802$ cm^{-1}, $B = 1.1 \times 10^5$ cm^{-1}, and $C = 0.500$ for the series of S_1 state energies and $A = 10\,955$ cm^{-1}, $B = 1.1 \times 10^5$ cm^{-1}, and $C = 2.020$ for the S_2 state energies. The *A* parameter represents the energy of the states in the long chain limit, *i.e.* when *N* goes to infinity. The *A* value of 10 955 cm^{-1} for the S_2 states of the spheroidene analogs is roughly 5000 cm^{-1} lower than that found by Kohler for the substituted polyenes but virtually indistinguishable from the value of 10 980 cm^{-1} found by Andersson and Gillbro[24] for the long-chain limit of the β-carotene analogs. Likewise, a fit of the $A + B/(N + C)$ equation to the S_1 energies for the

TABLE 2: Fluorescence Quantum Yields, ϕ_c, Radiative Rate Constants, k_r, Natural Lifetimes, τ_0, and Nonradiative Rate Constants, k_{ic}, of the S_2 (1^1B_u) States of Spheroidene and Its Analogs[a]

sample		$\phi_c/10^{-5}$	$k_r/10^9$ s^{-1}	τ_0/ns	$k_{ic}/10^{13}$ s^{-1}
3,4,7,8-tetrahydrospheroidene	**1**	12.6 ± 1.9	0.984 ± 0.009	1.020 ± 0.009	0.78 ± 0.12
3,4,5,6-tetrahydrospheroidene	**2**	22 ± 5	1.105 ± 0.009	0.911 ± 0.008	0.51 ± 0.11
3,4-dihydrospheroidene	**3**	27 ± 3	1.150 ± 0.008	0.869 ± 0.006	0.42 ± 0.05
spheroidene	**4**	12.0 ± 2.5	0.86 ± 0.04	1.16 ± 0.05	0.72 ± 0.15
5′,6′-dihydro-7′,8′-didehydrospheroidene	**5**	6.2 ± 2.0	0.74 ± 0.05	1.35 ± 0.10	1.2 ± 0.4
7′,8′-didehydrospheroidene	**6**	2.87 ± 0.15	0.72 ± 0.06	1.40 ± 0.11	2.5 ± 0.5
1′,2′-dihydro-3′,4′,7′,8′-tetradehydrospheroidene	**7**	3.05 ± 0.07	0.63 ± 0.06	1.60 ± 0.14	2.0 ± 0.4

[a] The uncertainties in the ϕ_c values are derived from the standard deviations from the mean values of several determinations. The uncertainties in k_r and τ_0 were propagated from the estimated uncertainties of the variables in the Stickler−Berg equation (eq 4), which is a function of the fluorescence intensity, $I(\nu)$, and molar absorptivities, $\epsilon(\nu)$, of the molecules. The uncertainties in k_{ic} were propagated from the uncertainties in ϕ_c and k_r. The ϕ_c values were measured according to the expression given in eq 1. The k_{ic} values were calculated from the ϕ_c and k_r values using eq 3.

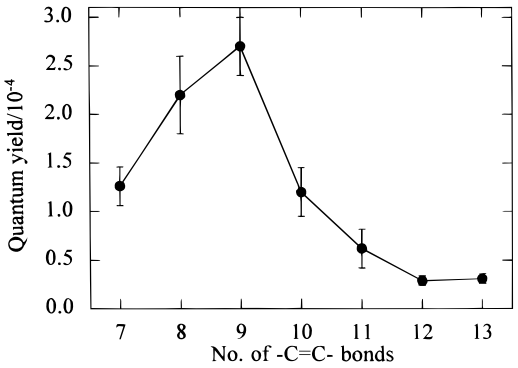

Figure 8. S_2 fluorescence quantum yields for spheroidene and its analogs. The error bars represent the uncertainties calculated from the standard deviations from the mean values of at least two trials, and, in each trial, the emissions at two or more wavelengths of excitation were measured.

spheroidene given in Table 1 and Figure 7 yielded a long-chain limiting energy for the 2^1A_g state of 3802 cm^{-1}. This is very close to the 3470 cm^{-1} value obtained by Andersson and Gillbro[24] for the long-chain limit of the β-carotene analogs but significantly lower than the value of 8550 cm^{-1} obtained by Kohler for the substituted polyenes. Undoubtedly, the methyl group substituents located along the conjugated chain of carotenoids, which are not present in the model polyenes, are perturbing the electron distribution of the electronic states in such a way that the state energies of carotenoids are significantly stabilized compared to those of the polyene systems.

The Quantum Yields of S_2 Emission. As seen in Figure 8 the S_2 fluorescence quantum yields increase as the extent of conjugation increases from seven to nine double bonds and then decrease as the extent of conjugation is increased further. The data for the S_1 and S_2 state energies presented in Figure 7 show that the energies of both states decrease with increasing π-electron conjugation, but the S_1 state energy decreases faster. This leads to a widening S_2-S_1 energy gap with increasing chain length. It is interesting to ask whether these changes in the S_1 and S_2 energies alone could account for the fact that the S_2 emission quantum yield for this series of spheroidene analogs reaches a maximum at nine carbon−carbon double bonds, or whether, for some of the molecules, other excited states into which internal conversion may occur must be invoked to rationalize this behavior. The quantum yield of emission, ϕ_c, from the S_2 state is related to the rate constants for radiative and nonradiative decay by the expression

$$\phi_c = \frac{k_r}{k_r + k_{ic}} \tag{3}$$

where k_r is the radiative rate constant and k_{ic} is the nonradiative rate constant describing internal conversion between the S_2 and S_1 states. Internal conversion occurring directly between the S_2 and S_0 states is assumed to be much less important owing to a larger energy gap between S_2 and S_0 compared to that between S_2 and S_1. k_r can be determined from the reciprocal of the natural lifetime, τ_0, on the basis of the Stickler−Berg equation[30]

$$k_r = 1/\tau_0 = 2.880 \times 10^{-9}\, n^2 \frac{\int I(\nu)\, d\nu}{\int \nu^{-3} I(\nu)\, d\nu} (g_l/g_u) \int \epsilon(\nu)\, d \ln \nu \tag{4}$$

where $I(\nu)$ and $\epsilon(\nu)$ are the fluorescence intensity and molar absorptivity, respectively, at the frequency, ν, given in cm^{-1} units. g_l and g_u are the degeneracies of the lower and upper states, and n is the refractive index of the medium. With the exception of spheroidene[31] (**4**), the molar absoptivities of the compounds studied here have never been determined. Therefore, in the calculation of the k_r values for the spheroidene analogs, the known molar absorptivities of carotenoids having the same extents of conjugation as the molecules in the present series were used. The molecules were ζ-carotene[31] for 3,4,7,8-tetrahydrospheroidene (**1**), neurosphorene[31] for 3,4-dihydrospheroidene (**3**), rhodopin[31] for 5′,6′-dihydro-7′,8′-didehydrospheroidene (**5**), anhydrorhodovibrin[31] for 7′,8′-didehydrospheroidene (**6**), and spirilloxanthin[31] for 1′,2′-dihydro-3′,4′,7′,8′-tetradehydrospheroidene (**7**). Because no carotenoid with a similar chromophore as 3,4,5,6-tetrahydrospheroidene (**2**) was found, its molar absorptivity was approximated as the average of the molar absorptivities of the values used for compounds **1** and **3**. For spheroidene and its analogs, the radiative rate constants were found generally to decrease with the extent of π-electron conjugation in the carotenoid chain. (See Table 2.) From the values of the quantum yields, ϕ_c, and the calculated k_r values, the k_{ic} values can be deduced from eq 3. The k_{ic} values deduced in this manner are given in the last column of Table 2. For the molecules in this series, only the value of k_{ic} from spheroidene has been experimentally determined. It has been measured from fluorescence up-conversion experiments to be 5×10^{12} s^{-1}.[32] This is very close to the 6.8×10^{12} s^{-1} value deduced here. Another measurement of k_{ic} for spheroidene obtained from transient absorption techniques gave a similar value of 3.1×10^{12} s^{-1}.[14]

In order to test whether a change in the rate of internal conversion for the $S_2 \rightarrow S_1$ transition, brought about by a change in the S_2-S_1 energy gap with the extent of π-electron conjugation, could account for the maximum in the series of S_2 quantum yields observed in Figure 8, the $k_{ic}(S_2 \rightarrow S_1)$ values for the carotenoids other than spheroidene were calculated from the energy gap law given in eq 2. The values for the rate constants

TABLE 3: Energy Gaps, ΔE, and Calculated Fluorescence Quantum Yields, ϕ_c(calc), of the S_2 (1^1B_u) States of Spheroidene and Its Analogs[a]

sample		$\Delta E(S_2-S_1)/cm^{-1}$	k_{ic}(calc)/10^{13} s^{-1}	ϕ_c(calc)/10^{-5}
3,4,7,8-tetrahydrospheroidene	**1**	5100 ± 600	1.2 ± 0.6	8 ± 4
3,4,5,6-tetrahydrospheroidene	**2**	5600 ± 600	0.8 ± 0.4	13 ± 7
3,4-dihydrospheroidene	**3**	5900 ± 600	0.6 ± 0.3	19 ± 10
spheroidene	**4**	6140 ± 400	(0.50 ± 0.12)[b]	17 ± 4
5′,6′-dihydro-7′,8′-didehydrospheroidene	**5**	6330 ± 400	0.46 ± 0.22	16 ± 8
7′,8′-didehydrospheroidene	**6**	6470 ± 400	0.47 ± 0.23	15 ± 8
1′,2′-dihydro-3′,4′,7′,8′-tetradehydrospheroidene	**7**	6580 ± 400	0.39 ± 0.19	15 ± 7

[a] The ΔE values were obtained from the fitted curves represented in Figure 7. Except for the value for spheroidene which is given in parentheses and was measured by experiment, the k_{ic}(calc) values have been calculated from these ΔE values and the energy gap law given in eq 2 in the text. The calculated quantum yields were based on eq 3 from the text and used the radiative rate constants, k_r, given in Table 2 evaluated using the Sticker−Berg expression (eq 4). The uncertainties in the k_{ic}(calc) and ϕ_c(calc) values were propagated from the precisions in the determination of k_r and the energy gaps, ΔE. [b] Experimentally determined value from Ricci et al.[29]

could only be approximated here owing to the fact that the parameters needed to evaluate eq 2 for the molecules in the spheroidene series are not known. Nevertheless, using the k_{ic} value of $(0.50 \pm 0.12) \times 10^{13}$ s^{-1} obtained by Ricci *et al.*[32] for spheroidene, the parameters needed to evaluate eq 2 for $k_{ic}(S_2 \rightarrow S_1)$ were estimated for the six analog compounds. From these parameters and the S_2-S_1 energy gaps (see Table 3), values of k_{ic} were calculated. These are denoted k_{ic}(calc) to distinguish them from the values of k_{ic} deduced from the quantum yields and given in Table 2. The k_{ic}(calc) values are given in Table 3. These were then substituted into the quantum yield expression given in eq 3 along with the values obtained for k_r according to eq 4. It was found that the new values of the quantum yields, ϕ_c(calc), calculated in this manner directly from a consideration of the rate constants of internal conversion for the $S_2 \rightarrow S_1$ transitions, increase as the π-electron conjugated chain length increases from 7 to 9 carbon−carbon double bonds and then decrease as the extent of π-electron conjugation is increased from 9 to 13 carbon−carbon double bonds. (See Table 3.) At this level of approximation it is not surprising that the calculated quantum yields, ϕ_c(calc), given in Table 3 do not agree perfectly with the experimentally determined quantum yields, ϕ_c, given in Table 2. However, this analysis does show that with increasing extent of π-electron conjugation, the different energy dependencies of k_r and k_{ic} can produce among this series of compounds a maximum S_2 emission quantum yield for 3,4-dihydrospheroidene, as is experimentally observed. Although other excited electronic states have been suggested to be close in energy to S_2,[33−37] it is not necessary to invoke internal conversion between S_2 and them for selective carotenoids in this series, to account for the trends observed in these data. It has been suggested that fast relaxation from the fluorescent $^1B_u^+$ state to a $^1B_u^-$ state followed by a slower relaxation between the $^1B_u^-$ state and the low-lying $^1A_g^-$ state is required from symmetry considerations for relaxation to S_1.[36,37] The above analysis shows that the trends in the quantum yields can be accounted for simply by a consideration of the energies and dynamics of only two low-lying excited states, S_1 (2^1A_g or $^1A_g^-$) and S_2 (1^1B_u or $^1B_u^+$).

Implications for Energy Transfer from Carotenoids to Bacteriochlorophylls in Photosynthesis. There are two important excited states of bacteriochlorophyll that can act as potential acceptors of the excitation energy from carotenoids. These are the states associated with the Q_x and Q_y transitions of bacteriochlorophyll. In the B800-850 antenna complex from purple photosynthetic bacteria, the Q_x transitions appear at about 590 nm (16 900 cm^{-1}) and the Q_y transitions occur either near 800 nm (12 500 cm^{-1}) or 850 nm (11 800 cm^{-1}). As described in detail in this paper, carotenoids also posses two low-lying excited states from which energy transfer can originate. These are the S_1 (2^1A_g) and the S_2 (1^1B_u) states. The structure of the B800-850 complex from *Rhodopseudomonas acidophila* 10050 shows that both the B800 and B850 bacteriochlorophylls are in van der Waals contact with the protein-bound carotenoid.[38] Until recently, it has generally been accepted that $S_2 \rightarrow S_1$ ($1^1B_u \rightarrow 2^1A_g$) internal conversion is so rapid that there would be little possibility of transfer to the bacteriochlorophyll originating from the S_2 state of the carotenoid. However, Shreve *et al.*[14] using femtosecond time-resolved optical spectroscopy have demonstrated that after excitation of the carotenoid, excited states of bacteriochlorophyll are formed in the same (∼200 fs) time domain as the S_2 state of the carotenoid decays. This is convincing evidence that transfer from the S_2 state of the carotenoid to bacteriochlorophyll occurs. Also, Andersson *et al.*[39] provided data from fast transient optical studies on *Chromatium purpuratum* that was consistent with energy transfer occurring directly from the B_u^+ state of the carotenoid, okenone, to the Q_x state of BChl. Precisely how much energy absorbed by the carotenoid is partitioned to bacteriochlorophyll via the S_2 state of a carotenoid and how much is transferred via S_1 is not completely understood, but undoubtedly it depends on the specific carotenoid and the complexion of its energy states. The probability of energy transfer from the S_2 state of the carotenoid may be enhanced for the longer chromophore carotenoids because the S_2 lifetime is longer for the more extensively conjugated molecules. This occurs because the S_2-S_1 energy gap widens with the extent of π-electron conjugation in the molecule. (See Figure 6). The rate of $S_2 \rightarrow S_1$ ($1^1B_u \rightarrow 2^1A_g$) internal conversion would then decrease according to the energy gap law and allow a higher probability of energy transfer from the S_2 state of the carotenoid to bacteriochlorophyll. The mechanism of energy transfer from the carotenoid to bacteriochlorophyll is expected to depend on which electronic state of the carotenoid acts as the energy donor. If the S_1 (2^1A_g) state is the donor, then the Dexter (exchange) mechanism[4] is more probable than the Coulomb mechanism[7] because of the vanishingly small transition dipole moment associated with the $S_0 \rightarrow S_1$ ($1^1A_g \rightarrow 2^1A_g$) transition. If the S_2 (1^1B_u) state is the donor, then the Coulomb mechanism may be more important. The Förster mechanism[3] is probably not operating in either of these cases due to the extremely fast dynamics of internal conversion between the excited singlet states and the ground state and the correspondingly low fluorescence quantum yields of the carotenoids.

It is known that carotenoids having conjugated chain lengths longer than spheroidene, in general, have lower efficiencies of energy transfer to the BChl.[2] For example, rhodopin, which has 11 conjugated carbon−carbon double bonds, bound in the B800-850 complex of *Rh. acidophila* transfers energy to bacteriochlorophyll with only ∼50% efficiency.[40,41] Spirilloxanthin, which has 13 carbon−carbon double bonds, in the B880 complex of *Rhodospirillum rubrum* transfers energy to bacte-

riochlorophyll with ~30% efficiency.[42] Spheroidene, with 10 carbon−carbon double bonds, in the antenna complex of *Rb. sphaeroides* wild type strain 2.4.1 transfers energy to bacteriochlorophyll with close to 90% efficiency. [28−43] It was previously suggested[44] that compared to the shorter (9 and 10 carbon−carbon double bonds) carotenoids, the faster rates of internal conversion from the S_1 (2^1A_g) states for the longer chromophore (11−13 carbon−carbon double bonds) carotenoids would compete more effectively with energy transfer to bacteriochlorophyll, thereby lowering the overall efficiency of energy transfer. Yet, another important factor controlling energy transfer is spectral overlap. For transfer out of the S_2 state, this would be primarily between the $1^1B_u \rightarrow 1^1A_g$ emission profile of the carotenoid and the Q_x absorption of the bacteriochlorophyll. For transfer from the S_1 state of the carotenoid, the dominant spectral overlap occurs between the $2^1A_g \rightarrow 1^1A_g$ emission band from the carotenoid and the Q_y absorption of the bacteriochlorophyll. The lower energy transfer efficiency for the longer chromophore carotenoids could result from the lack of spectral overlap between the S_1 state emission from the carotenoid and the Q_y absorption of the bacteriochlorophyll. This is evident from the S_1 energy determined here for 1′,2′-dihydro-3′,4′,7′,8′-tetradehydrospheroidene. This molecule has 13 carbon−carbon double bonds and is the longest in the series of molecules studied here. The S_1 energy for this molecule is predicted from eq 2 to be essentially isoenergetic at ~11 800 cm^{-1} with the 850 nm absorbing bacteriochlorophyll in the B800-850 complex. Owing to the large Stokes shift associated with the S_1 emission from carotenoids,[12] the spectral overlap with the B850 bacteriochlorophyll absorption would be much less for 1′,2′-dihydro-3′,4′,7′,8′-tetradehydrospheroidene than for spheroidene.[44] This, along with the enhanced decay dynamics of the S_1 states of the longer chromophore carotenoids compared to the shorter systems, could be the major contributing factor in the diminished capacity of the long chromophore carotenoids to transfer energy to bacteriochlorophyll.

If either of these factors, the enhanced decay dynamics of the S_1 states of the longer chromophore carotenoids or the decreased spectral overlap between the S_1 state emission from the long carotenoid and the Q_y absorption of the bacteriochlorophyll, are at least partially responsible for the lower overall efficiencies of the energy transfer in complexes containing those molecules, energy transfer from the S_2 state does not appear to compensate fully for the loss. Further studies of the dynamics of the photochemistry of carotenoids and the efficiencies of energy transfer to bacteriochlorophyll for the molecules bound in pigment−protein complexes *in vivo* will be needed to elucidate which of these factors is most important in controlling light harvesting in photosynthetic antenna.

Acknowledgment. This work was supported by grants to H.A.F. from the National Institutes of Health (GM-30353), the Human Frontier Science Program, the United States Department of Agriculture (92-37306-7690), and the University of Connecticut Research Foundation and to J.L. from the Human Frontier Science Program and the Netherlands Foundation of Chemical Research (SON), which is financed by the Netherlands Organization for the Advancement of Pure Research (NWO). The work at Argonne National Laboratory was supported by the Office of Basic Energy Sciences, Division of Chemical Sciences, U.S. Department of Energy, under Contract W-31-109-Eng-38.

References and Notes

(1) Cogdell, R. J.; Frank, H. A. *Biochim. Biophys. Acta* **1987**, *895*, 63.

(2) Frank, H. A.; Cogdell, R. J. In *Carotenoids in Photosynthesis*; Young, A., Britton, G., Eds.; Chapman and Hall: London, 1993; Chapter 8.

(3) Förster, Th. *Ann. Phys.* **1948**, *2*, 55.

(4) Dexter, D. L. *J. Chem. Phys.* **1953**, *21*, 836.

(5) Davydov, A. S. *Theory of Molecular Excitons* (translated by M. Kasha and M. Oppenheimer, Jr.); McGraw-Hill: New York, 1962.

(6) Nagae, H.; Kikitani, T.; Katoh, T.; Mimuro, M. *J. Chem. Phys.* **1993**, *98*, 8012.

(7) Kasha, M. *Radiat. Res.* **1963**, *20*, 55.

(8) Hudson, B. S.; Kohler, B. E.; Schulten, K. In *Excited states*; Lim, E. C., Ed.; Academic Press: New York, 1982; Vol. 6, p 22.

(9) Hudson, B. S.; Kohler, B. E. *Synth. Met.* **1984**, 9, 241.

(10) Orlandi, G.; Zerbetto, F.; Zgierski, M. Z. *Chem. Rev.* **1991**, *91*, 867.

(11) Petek, H.; Bell, A. J.; Christensen, R. L.; Yoshihara, K. *J. Chem. Phys.* **1992**, *96*, 2412.

(12) DeCoster, B.; Christensen, R. L.; Gebhard, R.; Lugtenburg, J.; Farhoosh, R.; Frank, H. A. *Biochim. Biophys. Acta* **1992**, *1102*, 107.

(13) Frank, H. A.; Farhoosh, R.; Gebhard, R.; Lugtenburg, J.; Gosztola, D.; Wasielewski, M. R. *Chem. Phys. Lett.* **1993**, *207*, 88.

(14) Shreve, A. P.; Trautman, J. K.; Frank, H. A.; Owens, T. G.; Albrecht, A. C. *Biochim. Biophys. Acta* **1991**, *1058*, 280.

(15) Andersson, P. O.; Bachilo, S. M.; Chen, R. L.; Gillbro, T. *J. Phys. Chem.* **1995**, *99*, 16199.

(16) Gebhard, R.; van Dijk, J. T. M.; van Ouwerkerk, E.; Boza, M. V. T. J.; Lugtenburg, J. *Recl. Trav. Chim. Pays-Bas* **1991**, *110*, 459.

(17) Van der Hoef, K.; Lugtenburg, J. To be published.

(18) Berlman, I. B. *Handbook of fluorescence spectra of aromatic molecules*; Academic Press: New York, 1965; p 175.

(19) Benfey, D. P.; Brown, D. C.; Davis, S. J.; Piper, L. G.; Foutter, R. F. *Appl. Opt.* **1992**, *31*, 7034.

(20) Demas, J. N.; Crosby, G. A. *J. Phys. Chem.* **1971**, *75*, 991.

(21) Frank, H. A.; Cua, A.; Chynwat, V.; Young, A.; Gosztola, D.; Wasielewski, M. R. *Photosynth. Res.* **1994**, *41*, 389.

(22) Cua, A. Photochemistry and photophysics of carotenoids in photosynthesis. Ph.D. Dissertation, University of Connecticut, 1996.

(23) Englman, R.; Jortner, J. *Mol. Phys.* **1970**, *18*, 145.

(24) Andersson, P. O.; Gillbro, T. *J. Chem. Phys.* **1995**, *103*, 2509.

(25) Bixon, M.; Jortner, J.; Cortes, J.; Heitele, H.; Michel-Beyerle, M. E. *J. Phys. Chem.* **1994**, *98*, 7289.

(26) Frank, H. A.; Chynwat, V. *Chem. Phys.* **1995**, *194*, 237.

(27) Wasielewski M. R.; Johnson, D. G.; Bradford, E. G.; Kispert, L. D. *J. Chem. Phys*. **1989**, *91*, 6691.

(28) Cogdell, R. J.; Andersson, P. O.; Gillbro, T. *J. Photochem. Photobiol. B* **1992**, *15*, 105.

(29) Kohler, B. E. *J. Chem. Phys.* **1990**, *93*, 5838.

(30) Strickler, S. J.; Berg, R. A. *J. Chem. Phys.* **1962**, *37*, 814.

(31) Britton, G. In *Carotenoids*; Britton, G., Liaaen-Jensen, S., Pfander, H., Eds.; Birkhauser Verlag: Basel, 1995; Vol. 1B, Chapter 2.

(32) Ricci, M.; Bradforth, S. E.; Jimenez, R.; Fleming, G. R. *Chem. Phys. Lett.*, in press.

(33) Tavan, P.; Schulten, K. *J. Chem. Phys.* **1986**, *85*, 6602.

(34) Tavan, P.; Schulten, K. *Phys. Rev. B* **1987**, *36*, 4337.

(35) Van Beek, J. B.; Kajzar, F.; Albrecht, A. C. *J. Chem. Phys.* **1991**, *95*, 6400.

(36) Watanabe, Y.; Kameyama, T.; Miki, Y.; Kuki. M.; Koyama, Y. *Chem. Phys. Lett.* **1993**, *206*, 62.

(37) Kuki, M.; Nagae, H.; Cogdell, R. J.; Shimada, R.; Koyama, Y. *Photochem. Photobiol.* **1994**, *59*, 116.

(38) McDermott, G.; Prince, S. M.; Freer, A. A.; Hawthornthwaite-Lawless, A. M.; Papiz, M. Z.; Cogdell, R. J.; Isaacs, N. W. *Nature* **1995**, *374*, 517.

(39) Andersson, P. O.; Cogdell, R. J.; Gillbro, T. O. Abstracts of the 6th Congress of the European Society for Photobiology, Cambridge, 1995; p 4.

(40) Angerhofer, A.; Cogdell, R. J.; Hipkins, M. F. *Biochim. Biophys. Acta* **1986**, *848*, 333.

(41) Chadwick, B. W.; Zhang, C.; Cogdell, R. J.; Frank, H. A. *Biochim. Biophys. Acta* **1987**, *893*, 444.

(42) Noguchi, T.; Hayashi, H.; Tasumi, T. *Biochim. Biophys. Acta* **1990**, *1017*, 280.

(43) Cogdell, R. J.; Hipkins, M. F.; MacDonald, W.; Truscott, T. G. *Biochim. Biophys. Acta* **1981**, *634*, 191.

(44) Frank, H. A.; Farhoosh, R.; Aldema, M. L.; DeCoster, B.; Christensen, R. L.; Gebhard, R.; Lugtenburg, J. *Photochem. Photobiol.* **1993**, *57*, 49.